# Geologic characterization of nonconformities using outcrop and whole-rock core analogues: hydrologic implications for injection-induced seismicity

5  Elizabeth S. Petrie[1], Kelly K. Bradbury[2], Laura Cuccio[2], Kayla Smith[2], James P. Evans[2], John P. Ortiz[4,5], Kellie Kerner[3], Mark Person[3], and Peter Mozley[3]

[1]Western Colorado University, Geology Department, 1 Western Way, Gunnison, 81231, USA

[2]Utah State University, Geology Department, 4505 Old Main Hill, Logan, UT 84322-4505, USA

10  [3]New Mexico Institute of Mining and Technology, 801 Leroy Pl Socorro, NM 87801, USA

[4]Computational Earth Science Group, Los Alamos National Laboratory, Los Alamos, NM 87544, USA

[5]Johns Hopkins University, Department of Environmental Health and Engineering, 3400 N. Charles St., Baltimore, MD 21218, USA

*Correspondence to*: Elizabeth S. Petrie (epetrie@western.edu)

15  **Abstract.** The occurrence of induced earthquakes in crystalline rocks kilometres from deep wastewater injection wells poses questions about the influence nonconformity contacts have on the downward and lateral transmission of pore fluid pressure and poroelastic stresses. We hypothesize that structural and mineralogical heterogeneities at the sedimentary-crystalline rock nonconformity control the degree to which fluids, fluid pressure, and associated poroelastic stresses are transmitted over long distances across and along the nonconformity boundary. We examined the spatial distribution of physical and chemical

20  heterogeneities in outcrops and whole-rock core samples of the great nonconformity in the midcontinent of the United States, capturing a range of tectonic settings and rock properties that we use to characterize the degree of historical fluid communication and the potential for future communication. We identify three end-member nonconformity types that represent a range of properties that will influence direct fluid pressure transmission and poroelastic responses far from the injection site. These nonconformity types vary depending on whether the contact is sharp and minimally altered, or if it is dominated by

25  phyllosilicates or secondary non-phyllosilicate mineralization. We expect the rock properties associated with the presence or absence of secondary non-phyllosilicate mineralization and phyllosilicates to either allow or inhibit fractures to cross the nonconformity, thus impacting the permeability of the nonconformity zone. Our observations provide geologic constraints for modelling fluid migration and the associated pressure communication and poroelastic effects at large-scale disposal projects

by providing relevant subsurface properties and much needed data regarding common alteration minerals that may interact

30 readily with brines or reactive fluids.

## 1 Introduction

Deep wastewater injection near the nonconformity between the Phanerozoic sedimentary sequence and Proterozoic crystalline basement in the mid-continent United States (Sloss, 1963) is the primary means by which produced formation fluids are

35 disposed of in Class II injection wells (Murray, 2015). Increased rates of seismicity in this region are associated with large volumes of wastewater injection (Ellsworth et al., 2015; Keranen et al., 2013; Nicholson and Wesson, 1990; Petersen et al., 2016; Zhang et al., 2013), reduction of friction on pre-existing faults, and pressure diffusion away from the injection point controlled by the permeability structure of the rocks in the subsurface (Goebel and Brodsky, 2018; Yehya et al., 2018). Recent mid-continent seismicity nucleates on faults in crystalline rocks km's from injection sites (Keranen et al., 2014; Weingarten et

40 al., 2015; Zhang et al., 2016), and spans timescales of months to years' post-injection, indicating that pore-fluid pressures and/or poroelastic loads are transmitted across or along the nonconformity zone or through connected fracture systems in the crystalline rocks (Ortiz et al., 2019). The depths of seismicity (up to 11 km) at some injection sites suggest that crystalline basement permeability is perhaps moderate to high ($10^{-16}$ to $10^{-14}$ m$^2$; (Zhang et al., 2016) and is dynamically increased by elevated fluid pressures (Rojstaczer, 2008).

45 The nonconformity zone is the rock volume surrounding the nonconformable contact. This zone may range from diffuse to sharp, be phyllosilicate rich, or dominated by non-phyllosilicate secondary minerals. Each contact type observed in this study has a range of mineralized textures and structural discontinuities. Characterizing variations in rock properties at the nonconformity zone is critical for safe implementation of deep fluid injection, as the dimensions and hydraulic properties of the rocks in the nonconformity zones impact the subsurface flow regimes (Ortiz et al., 2019). Due to weathering, deformation,

50 diagenesis and fluid-rock interactions, the nonconformity zone may be hydraulically heterogeneous at the mm to 10's m scales and influence the migration of fluid and fluid pressures away from the injection well. The lithologic character of the nonconformity zone has implications for hydraulically connected regions by allowing direct fluid communication, changes in pore fluid pressure, and/or poroelastic loads.

Numerical modelling of fluid flow and/or loading stresses associated with poroelastic effects across nonconformities indicate

55 that: 1) the presence of a high-storativity, low-permeability basal seal reduces potential for basement induced earthquakes; 2) poroelastic effects can trigger seismicity far away from the injection location; 3) the presence of conductive faults, including those that cut the nonconformity and those that are isolated in the basement can provide direct fluid or fluid pressure pathways, and 4) permeable cross-nonconformity faults may exhibit high rates of seismicity (Chang and Segall, 2016; Goebel and Brodsky, 2018; Ortiz et al., 2019; Yehya et al., 2018; Zhang et al., 2013).

60    We document the lithology and structural features of the rocks on either side of the nonconformity in outcrops and whole-rock
      core to characterize the range of rock types and geologic settings associated with the contact and identify any evidence of past
      cross-contact fluid flow. The sites evaluated here provide geological and hydrogeological analogues that aid in understanding
      controls on cross-contact fluid flow and the impacts deep circulating fluids may have on altering rock properties at depth
      (Oliver et al., 2006). Because pressure diffusion and fluid migration depend on the permeability structure at a given location,
65    our work can be used to improve hydrogeologic models that test the impact of lithologic changes and cross-nonconformity
      fractures on the transmission of pore fluids and/or poroelastic stress.

      In this paper we characterize nonconformities that are associated with Precambrian granite, gabbro, gneiss, and schists, and
      are overlain by porous sedimentary rocks. We present data on the mineralogic and structural heterogeneities observed in
      outcrop and core, and these observations serve as proxies for variation in mineral alteration and deformation at the
70    nonconformity which may impact the migration of fluids along and across the contact.

## 2 Characterization of the nonconformity

      Given the recognized importance of direct fluid transmission, variation in pressure, and poroelastic loads on induced seismicity
      (Chang and Segall, 2016; Ortiz et al., 2019; Yehya et al., 2018; Zhang et al., 2013), we provide an overview of rock properties
      observed at the nonconformity using integrated outcrop-based studies in Michigan and New Mexico, and analyses of core from
75    Michigan, Minnesota and Nebraska (Fig. 1).

### 2.1 Methods

      To describe the nonconformity zone, we analyse outcrop sites and core samples. The outcrop sites are from the southern shore
      of Lake Superior, Michigan, where the late Proterozoic Jacobsville Sandstone overlies Archean and Proterozoic crystalline
      rocks, and the eastern Sangre de Cristo Mountains, New Mexico, where Devonian to Mississippian Espiritu Santo Formation
80    overlies the Proterozoic Gallinas Canyon gneiss. We examine core from Nebraska that samples the Cambrian Lamotte
      Sandstone and its contact with the granitic Yavapai-Mazatzal Precambrian complex (Whitmeyer and Karlstrom, 2007), core
      from the Michigan basin that samples Precambrian granitoid gneiss near the Grenville Front, overlain by the Cambrian Mt.
      Simon Sandstone, and core from south-eastern Minnesota that samples Precambrian metagabbro, diabase, and metadiorite also
      overlain by the Cambrian Mt. Simon Sandstone.
85    To describe rock properties observed at the nonconformity interface zone we use a variety of micro- to meso-scale methods
      including detailed lithological and structural logging of outcrop and core, optical petrography and x-ray diffraction (XRD)
      mineralogic studies, whole-rock x-ray fluorescence (XRF) elemental analysis, and gas permeability measurements.

## 2.2 Results

### 2.2.1 Lake Superior, Michigan

90   Outcrops of the nonconformity between late Proterozoic Jacobsville Sandstone and early Proterozoic altered peridotite crystalline basement are exposed at Presque Isle and Hidden Beach along the southern shore of Lake Superior, Michigan (Lewan, 1972). At these localities the Jacobsville Sandstone (Hamblin, 1958) consists of a variably indurated pebble to cobble conglomerate and a lenticular planar to cross-bedded light red quartz arenite (Fig. 2).

At Presque Isle, a mineralized conglomerate is in direct contact with the underlying serpentinized peridotite or is transitionally

95   interbedded with the overlying sandstone (Fig. 2B). Where present, the low-porosity conglomerate consists of sub-angular to rounded chalcedony, gneiss, and greenstone cobble clasts with fine-grained, poorly sorted, hematite cemented angular quartz grains.

At Hidden Beach, poorly consolidated basal conglomerates of the Jacobsville Sandstone are in contact with the Precambrian Compeau Creek Gneiss. The quartz arenite consists of fine-grained, angular, moderately sorted quartz with some feldspar.

100   Distinctive near-vertical to bedding-parallel bleached fractures or reduction spots are associated with the lower Jacobsville Sandstone and are not observed to extend into the basement (Fig. 2C). Locally, basement-hosted slip surfaces are coated with epidote-iron oxide and roughly align with the vertical bleached fracture zones in the overlying Jacobsville Sandstone (Fig. 2C).

Optical petrography across the transition from red sandstone protolith to a bleached fracture zone at Hidden Beach reveals a

105   reduction in hematite grain coatings and cements. Whole-rock XRF analysis of the bleached areas of Jacobsville Sandstone indicates a minor depletion of $K_2O$, and a minor enrichment of $FeO$ and $MgO$, relative to the unaltered Jacobsville Sandstone (Figure 3). At Presque Isle, mineral alteration products in the conglomerate include nontronite, with trace zeolites and iron oxides (Fig. 3). The underlying serpentinized peridotite is black to brown, with abundant white carbonate mesh veinlets and localized stockwork jasperoid veins up to 10 cm wide. Jasperoid mineralization occurs along a few small faults that span the

110   contact.

### 2.2.2 Gallinas Canyon, New Mexico

Devonian to Mississippian carbonate and clastic rocks of the Espiritu Santo Formation deposited on the Proterozoic quartzo-feldspathic and amphibolitic gneiss, biotite schist, and granitic pegmatite (Lemen et al., 2015) are exposed along a 4-km long section in Gallinas Canyon, eastern Sangre de Cristo Mountains, New Mexico. The nonconformity is cut by cm- to m's -

115   displacement faults, where we characterize both the faulted and the adjacent un-faulted nonconformity zone (Hesseltine, 2019; Kerner, 2015). The carbonate and clastic rocks of the Espiritu Santo Formation include: 1-m thick massive, fine-grained, rounded to sub-rounded sandstone with calcite nodules, ~1- m of microcrystalline dolomite that transitions upward into a chert nodule limestone, interbedded mudstone and limestone and a massive microcrystalline limestone bed. A phyllosilicate-rich

zone directly below the nonconformity is approximately 60-cm thick and is a poorly lithified zone that marks the transition
120  from highly altered (weathering and hydrothermal alteration) to minimally altered crystalline rock (Fig. 4).

The predominant lithology of the crystalline basement is gneiss, with minor schist, pegmatitic granite, and basalt. Mineral
alteration is greatest directly below the nonconformity. This zone is enriched in sericite within feldspars, and clay minerals
(mixed with hematite and associated with replacement of micas) (Fig. 5). Where cut by faults the nonconformity-associated
phyllosilicates form a matrix that surrounds more rigid grains such as quartz, suggesting deformation in this unit was
125  accommodated by granular flow, a process associated with high pore-fluid pressure. Microscopic fracturing has occurred
within the crystalline basement, these fractures are mineralized with iron oxide, sericite, chert, and calcite. The majority of
fractures within the crystalline basement occur along weak grains such as sericitized feldspar and altered mica or cut across
quartz and feldspar grains. Authigenic calcite is rare within the crystalline basement, though commonly occurs as coarsely
crystalline calcite cement within grain fractures in feldspar and sericitized feldspar.

130  Fractures cut the altered crystalline basement locally and cataclasites are found throughout the fault core in crystalline basement
but are absent within protolith crystalline basement. Where faulted, the sedimentary rock damage zone includes large twinned
calcite grains in fracture-filling cements, and cataclasites that lie along the edges of the calcite veins. These cataclasites include:
pulverized quartz and feldspar grains, chert, pulverized protolith, as well as clay- and iron oxide-rich minerals. Quantitative
microprobe analyses of the carbonate and fine-grained matrix composition within the sedimentary and basement fault cores
135  reveals that all calcite vein elemental values have a slightly reduced level of iron and Mg substitution for Ca than the calcite
matrix. The fine-grained matrix within the sedimentary fault core is nearly pure silica, whereas the fine-grained matrix within
the crystalline basement fault core is aluminium-rich (Fig. 5).

### 2.2.3 R.C. Taylor 1 Core, Nebraska

Core from the R.C. Taylor 1 wildcat well was obtained in 1953 in south-central Nebraska. We examined a total of 19.2 m of
140  core recovered over the Cambrian Lamotte Formation sandstone and sheared Proterozoic granitoids in the Central Plains
Orogen of the Yavapai Province (Marshak et al., 2017; Sims, 1990; Whitmeyer and Karlstrom, 2007). The arkosic Lamotte
Formation, regionally called the Reagan and Sawatch Sandstones, is a fine-grained, well-sorted glauconitic sandstone (Fig. 6).
The basal Lamotte Formation is cut by quartz, calcite, dolomite, and iron-oxide veinlets. Iron-oxide veins cut quartz veins, and
both are cut by calcite veins, providing evidence for three mineralization events here (Fig. 7). Below the Lamotte Formation
145  is a phyllosilicate-rich zone composed of 40 cm thick highly altered basement shear zone that overlies a minimally altered
basement shear zone, both are comprised of fine crystalline sericitized feldspar and chlorite-rich shear zones, and overlie the
coarse-crystalline, minimally altered granitic basement containing some sericitized feldspar (Fig.7).

The altered basement shear zone is composed of quartz, feldspar, biotite, chlorite, and dolomite (Fig. 7). Quartz and feldspars
are disintegrated, well-developed chlorite, hematite and magnetite are altered from biotite, and granular disintegration has
150  resulted in clay development. Open pore-space occurs between host-rock grains and neoformed clays. The basement shear
zone is characterized by feldspar, quartz, mica, and the alteration minerals chlorite and dolomite (Fig. 7). The shear zones

contain fractures, slip surfaces, and S-C fabrics within chloritizied zones. The shear fabrics are cut by quartz, sparry calcite, iron-oxide and dolomite veins. The basal, moderately altered basement unit is a coarse-crystalline granite composed of feldspar, quartz, biotite, and hornblende (Fig. 7). Chlorite is present and associated with minor shear fabrics. Calcite, dolomite,

155  and quartz veins parallel and cross-cut the chlorite-rich shear fabrics and cut quartz and feldspar crystals (Fig. 7). In the coarse-crystalline granite altered feldspars contain sericite that has formed adjacent to twin planes. Veins of dolomite, calcite, and hematite occur in the lower 7 m of the Lamotte Formation and are observed through the underlying granitic shear zone covering 12.5 m of core.

### 2.2.4 CPC BD-139 Core, Michigan

160  The CPC BD-139 core, obtained in 1964 for the design of a brine disposal well, samples the contact between the Cambrian Mt. Simon Sandstone and Precambrian altered granitoid gneiss of the Grenville Front Tectonic Zone. We divide the CPC DB-139 core into three lithologic units: a laminated sandstone, a finely foliated gneiss, and a gneiss with sub-horizontal white veins. Both gneiss units have zones of dolomitization. The Mount Simon Sandstone reservoir is a unit of deep wastewater injection in Oklahoma and it is also targeted for $CO_2$ storage (Dewers et al., 2014). Measured porosity values of the Mount

165  Simon Sandstone range from 11-18% (Wisconsin Geological Natural History Survey, 2019).
Sandstone grains are rounded to sub-rounded and moderately to well-sorted. A discrete boundary separates the Mt. Simon Sandstone from the underlying altered granitoid gneiss (Fig. 8). The uppermost 30 cm of the basement is composed of tan, fine-grained, dolomite horizon which grades into a dark green foliated gneiss cut by pink sub-vertical fractures over a span of ~5 cm (Fig. 8). The basal meter of the Mt. Simon Sandstone is a tan, finely laminated arenite with minor amounts of iron-rich

170  clay. The quartzo-feldspathic granitoid gneiss near the contact contains the following alteration products: zeolites, vermiculite, and Fe-, Mn-oxides, and carbonates including dolomite (Fig. 9). Dolomitization of the basement host rock re-appears ~2 meters below the nonconformity. The original basement foliation is preserved and is associated with micrometer-scale crystalline dolomite grains, radiating silica crystals, and sub-horizontal calcite and dolomite veins (Fig. 9). Trace amounts of ankerite, clinochlore, and vermiculite are also present in the dolomitized basement rocks (Fig. 9).

175  **2.2.4 BO-1 Core, Minnesota**

The BO-1 core was originally collected in 1962 as part of an exploratory mining project in Fillmore County, southeast Minnesota (Gilbert, 1962).This core provides a continuous 300 m section of altered and mineralized rocks of lower Cambrian Mount Simon Sandstone overlying a Precambrian layered intrusive complex of altered and altered gabbro, other mafic intrusions and felsic dikes (Smith et al., 2019; Fig. 10). The crystalline basement rocks are part of the Northeast Iowa Intrusive

180  Complex and are hypothesized to be a part of the Midcontinent Rift System (Anderson, 2012) The BO-1 core is analogous to several geologic settings anticipated in the subsurface of midcontinent region where lower Cambrian to upper Ordovician rocks directly overly Precambrian mafic igneous rocks along the Great Unconformity (Gilbert, 1962; Mossler,

1995).Northwest trending fault systems near the borehole were identified by magnetic lineaments and are likely part of the regional NW-SE Belle Plaine Fault Zone (Drenth et al., 2015).

185    Sedimentary sequences in BO-1 extend to ~ 1.2 km where the nonconformity is marked by an ~ 12 cm zone of pervasive leaching and iron-hydroxide staining (goethite). Intense alteration extends into the basement rocks for ~ 21 m, with ~ 50 m of argillitic and propylitic alteration, multi-layered veins, and/or fracture mineralization observed to ~ 402 m depth (Fig. 10). Localized fault and fracture surfaces intersect the sampled basement core from within ~ 1 cm of the nonconformity contact and extend to 475.5 m, fracture density decreases with depth. Slip surfaces exhibit oblique to dip-slip slickenlines and range

190    from mm's to cm's thick and are either coated in clay or contain mineral infillings (±carbonate, ±silica, ±chlorite, ±iron-oxides).

The porous Mt. Simon Sandstone contains a ~ 0.5 meter zone of intense iron-hydroxide (goethite) alteration at the nonconformity (Fig. 10). This iron-hydroxide oxidized zone extends for several m's into the slightly altered and metamorphosed crystalline basement rock. From petrographic and X-ray diffraction analyses, we identify mineralogical

195    assemblages (Fig. 11; dolomite, siderite, iron-oxides, iron-hydroxides, illite, smectite, kaolinite-serpentinite, vermiculite) and textures that are indicative of weathering, diagenesis, and multiple episodes of fluid-rock interactions coupled with deformation within the broad ~ 50 m zone of intense alteration marked by the abundant structural discontinuities (Fig. 11).

Measured gas permeability values are highest above the nonconformity within the porous Mt. Simon sedimentary reservoir (up to 1000 millidarcy) and vary significantly from 0-500 millidarcy below the nonconformity contact, locally permeability

200    increases in direct correlation to the presence of structural discontinuities (Fig. 10).

## 3 Discussion

The nonconformities we examined range from sharp contacts to zones several m's thick and exhibit a range of mineralized textures and structural discontinuities. These include small faults, *in-situ* mineral growth, dissolution, recrystallization, foliations and veins that reflect mineralization or deformation at depth and are not the result of alteration due to weathering

205    alone.

We divide nonconformities into three types: Type 0 – a sharp contact between sedimentary strata and basement rocks (Hidden Beach); Type I – an interface dominated by phyllosilicates (Gallinas Canyon, and Nebraska core); and Type II – an interface dominated by non-phyllosilicate secondary mineralization (Michigan Basin core, BO-1 core, and Presque Isle).

We expect the non-fractured Type 0, I and II subtype nonconformities (Fig. 12) to each impact fluid migration and the

210    distribution of poroelastic stress differently. We note that all three nonconformity sub-types could promote long-distance lateral (along-nonconformity) fluid and/or pressure migration away from the borehole.

For Type 0, a sharp contact with minimal alteration (Fig. 12A), the non-conformity region is expected to prevent direct fluid pressure communication across the contact due to a significant contrast in rock permeabilities and would hinder cross-contact fluid migration while promoting migration parallel to the contact. The Type 0 contact type is observed elsewhere (Armstrong

and Carter, 2010; Easton and Carter, 1995), and has been observed at the Hidden Beach locality. At Hidden Beach a 0.3 to 1 m thick portion of poorly cemented basal Jacobsville conglomerate overlies the Archean Campeau Gneiss. The hydrogeologic impact of the unfractured Type 0 nonconformity type would likely be to distribute fluids laterally away from the injection site (Fig. 12A).

In the R.C. Taylor 1 core, a Type I nonconformity, the vein mineralogy and cross-cutting relationships provide evidence for cross-nonconformity flow. The altered basement shear zone is dominated by chlorite mineral foliations cut by brittle fractures and vein fill of iron-oxide, calcite, dolomite, and we observe porosity between neo-formed clays and rigid grains. Iron-oxides, calcite, dolomite, and quartz veins cut both the overlying Lamotte Formation and underlying crystalline basement (Fig. 12B). Repeated brittle failure and mineralization suggest that the altered shear zone is a zone of mechanical weakness that can be reactivated allowing development of fracture permeability. In the fractured nonconformities we note evidence for alteration as deep as 5 m below the nonconformity in the crystalline rocks (Duffin et al., 1989).

We observe mineralogic alteration across the nonconformity that impacts diffusivity and storativity.  At the Gallinas Canyon (Type I), Presque Isle and CPC BD-139 core (Type II), weathering and diagenetic alteration within the basement and/or diagenetic alteration of the sedimentary section above the basement results in low permeability barriers. At Gallinas Canyon fractures in the overlying sedimentary rock terminate in a relatively ductile phyllosilicate-rich altered zone. This alteration appears to have formed a barrier to cross-contact fluid flow by inhibiting fracture propagation. In such cases, nonconformities result in a poor hydrologic connection between the sedimentary section and deeper basement rocks.

Type II nonconformities (Fig. 12C) are mineralized contacts, and these contacts include secondary alteration minerals found within 10 cm to several m's below the nonconformity. The presence of these alteration minerals supports the hypothesis of direct fluid communication between sedimentary rocks and crystalline basement rocks.

At Presque Isle, a 0.3 to 1 m thick well-cemented (mineralized) conglomerate lies above the Precambrain serpentinized peridotite basement, and bleached fractures within the Jacobsville Sandstone do not cut the conglomerate. The mineralized contacts at Presque Isle and the CPC BD-139 core act as a mechanical barrier reducing the likelihood of fracture networks traversing the nonconformity.

The mineralization due to fluid-rock interactions at the Type II nonconformities suggests that deep fluid circulation occurs even without enhanced permeability from fractures (Fig. 12C). The mechanical/rheologic changes at these nonconformities could prevent brittle deformation but may be more influenced by poroelastic loads. The impact of these contacts on hydrogeologic properties is not yet well understood or modelled.

The structural elements and fluid-related alteration patterns observed in analogue sites support the hypothesis that the nonconformity interface zone influences or controls the potential for cross-contact fluid flow and distribution of fluids within the crust. Once fluids penetrate the basement, flow is likely controlled by fracture and fault systems and reactivation of pre-existing structures is possible. However, micro-porosity within basement rocks may enhance mineralogical changes over the long term and transmit fluids deeper in the basement while promoting short-term lateral migration along the nonconformity.

The impact the morphology of the nonconformity has on the downward propagation of fluid pressures into the crystalline basement has been shown by several numerical hydrogeologic studies (Ortiz et al., 2019; Segall and Lu, 2015; Yehya et al., 2018; Zhang et al., 2016). These models suggest that direct pore-fluid pressure communication (Ortiz et al., 2019; Segall and Lu, 2015; Yehya et al., 2018) and significant changes in poroelastic stress (Goebel and Brodsky, 2018; Zhang et al., 2016) can occur well way from the injection zones. Numerical models predict that nonconformities with through-going fractures distribute fluid deeper into the basement rocks and that direct pore pressure communication can destabilize faults at depth (Ortiz et al., 2019; Segall and Lu, 2015; Yehya et al., 2018). All the nonconformity types observed here are cut by structural discontinuities, and several possible contact sub-types exist within these 3 proposed end member scenarios (Fig. 12). Fractures, and especially fault zones, are expected to  distribute fluids and propagate fluid pressures to a greater depth regardless of nonconformity type (Yehya et al., 2018). Because nonconformity interface zones with pre-existing deformation fabrics may be preferential flow pathways that distribute fluid pressure away from the injection zone, high-permeability damage zones transmit fluid pressure to greater depths than non-conduit fault zones (Yehya et al., 2018). Our collective field and core observations document the occurrence of significant lateral variations in altered or mineralized zones that are associated with a relatively wide range of permeability values, and that alteration coupled with abundant structural discontinuities can result in relatively higher permeability that extends for 10's of m's both laterally and vertically into the crystalline basement rock below the nonconformity.

To illustrate effects of a reduced permeability above the nonconformity on fluid migration we compare three models of basal reservoir injection that consider continuous and discontinuous zones of altered low permeability rocks above the basement (Fig. 13). Each model run includes a 100 m-thick basal reservoir ($3\times10^{-15}$ m$^2$) underlain by 9.9 km of relatively low permeability ($k_x = k_z = 3\times10^{-17}$ m$^2$) crystalline basement rock. A 20 m-wide conduit-barrier fault ($k_z/k_x=105$; $k_z = 3 \times 10^{-10}$ m$^2$) is present in all simulations as is an injection well located 150 m from the fault zone. Wellhead pressures reached over 50 m excess hydraulic head after 4 days in response to 5000 m$^3$/day of continuous injection. The first model (Fig. 13A) is a Type 0 nonconformity, represented by a sharp contact between basement and overlying injection reservoir. In the second model simulation, a Type I nonconformity, we included a 20-m-thick, low-permeability ($k_x=k_z=3\times10^{-18}$ m$^2$) zone (Fig. 13B); this layer is 1 order of magnitude less permeable than the basement host rock and a further 1 order of magnitude less permeable in the fault core. The continuous low permeability zone reduces the permeability of the basement fault damage zone by 4 orders of magnitude, making the fault damage zone non-conductive. Pressure does not propagate into the crystalline basement although there was some diffusion of the 2-m excess hydraulic head front to depths $\leq$ 500 m. In the third simulation, a discontinuous low permeability zone is present (Fig. 13C). Where this zone is absent, the pressure front propagates into the basement along the fault damage zone to a depth of 2.5 km. The fault zone was not blocked by the low permeability zone, and elevated pore pressures propagated downward to depths of 2.5 km via the fault zone (Fig. 13C). Elevated fluid pressures likewise appeared to be forced down other areas where the low permeability zone pinches out, such as towards the right-hand side of Fig. 13C.

## 4 Conclusions

We define key rock types and structural elements of the nonconformity zone and split the analogue nonconformities into three end-member types. The geologic conditions associated with the nonconformities documented here can be used to help constrain the permeability architecture that impacts both diffusivity and storativity at and across the nonconformity. We expect these nonconformity types to either distribute fluid pressure away from the injection point or provide direct communication with basement rocks, distributing fluids to a greater depth across the nonconformity. We observe that fractures cut all nonconformity types and expect in these cases that changes in fluid pressure or poroelastic loads could result in triggered earthquakes within basement rocks (Chang and Segall, 2016; Zhang et al., 2013). Numerical modelling of Type 0 and Type I end members that include fault zones predict downward propagation of fluid pressure and changes to poroelastic loads. The data presented here can be used to improve model inputs for evaluation of cross-contact fluid and pressure communication whether through creation or modification of existing permeability or poroelastic pathways or through rheological changes associated with fluid-rock interactions. We show that *in-situ* conditions along the nonconformity zone vary, and observe common, localized, high permeability zones. The data from outcrop and core observations also suggest that injection of brines at depth may drive mineralogical alteration and potential fault zone weakening, these data can also be used to understand the impact that long-term storage of chemically reactive fluids has on rock properties. Our observations illustrate that the contact should not be treated as an impermeable barrier to fluid flow nor as one cut by faults of various permeabilities but should instead be evaluated on a site by site basis prior to injection of large fluid volumes.

## 5 Acknowledgements

This work was supported by collaborative NEHRP grants #G15AP00080 and #G15AP00081 awarded to Evans, Bradbury, Person, and Mozley, a Western State Colorado University Professional Activity Fund grant to Petrie, and a USGS-USU cooperative agreement #G17AC00345 to Bradbury and Evans. Additional student support obtained from student research grants from the Geological Society of America (GSA) awarded to Cuccio, Hesseltine, and Smith, the GSA Stephen E. Laubauch Structural Diagenesis Award to Smith, and a GDL Foundation grant to Cuccio.

# References

Anderson, R.: U.S. Geological Survey Airborne Study of Northeast Iowa, Iowa Geological & Water Survey., 2012.

Armstrong, D. K. and Carter, T. R.: The subsurface Palaeozoic stratigraphy of Southern Ontario, Ontario Geological Survey, Sudbury, Ontario., 2010.

Chang, K. and Segall, P.: Injection-induced seismicity on basement faults including poroelastic stressing, Journal of Geophysical Research: Solid Earth, 121(4), 2708–2726, 2016.

Dewers, T., Newell, P., Broome, S., Heath, J. and Bauer, S.: Geomechanical behavior of Cambrian Mount Simon Sandstone reservoir lithofacies, Iowa Shelf, USA, International Journal of Greenhouse Gas Control, 21, 33–48, doi:10.1016/j.ijggc.2013.11.010, 2014.

Drenth, B. J., Anderson, R. R., Schulz, K. J., Feinberg, J. M., Chandler, V. W. and Cannon, W. F.: what lies beneath: geophysical mapping of a concealed Precambrian intrusive complex along the Iowa–Minnesota border, Canadian Journal of Earth Sciences, 52, 279–293, doi:10.1139/cjes-2014-0178, 2015.

Duffin, M. E., Lee, M., Klein, G. D. and Hay, R. L.: Potassic diagenesis of Cambrian sandstones and Precambrian granitic basement in UPH-3 deep hole, Upper Mississippi Valley, USA, Journal of Sedimentary Research, 59(5), 1989.

Easton, R. M. and Carter, T. R.: Geology of the Precambrian basement beneath the Palaeozoic of southwestern Ontario, in Basement Tectonics 10, pp. 221–264, Springer., 1995.

Ellsworth, W. L., Llenos, A. L., McGarr, A. F., Michael, A. J., Rubinstein, J. L., Mueller, C. S., Petersen, M. D. and Calais, E.: Increasing seismicity in the U. S. midcontinent; implications for earthquake hazard (in Injection-induced seismicity), The Leading Edge, 34(6), 618–626, 2015.

Gilbert, R. C.: Final Report Minnesota Project (Area 4) Fillmore County, Minnesota, The New Jersey Zinc Company, Platteville Wisconsin., 1962.

Goebel, T. H. W. and Brodsky, E. E.: The spatial footprint of injection wells in a global compilation of induced earthquake sequences, Science, 361, 899–904, 2018.

Hamblin, W. K.: The Cambrian sandstones of northern Michigan, University of Michigan., 1958.

Hesseltine, G.: Micro- to Macro-Scale Structural and Lithological Architecture of Basal Nonconformities: Implications for Fluid Flow and Injection Induced Seismicity, MS, Utah State University, Logan, UT., 2019.

Keranen, K. M., H.M, S., G.A, A. and Cochran, E. S.: Potentially induced earthquakes in Oklahoma, USA: Links between wastewater injection and the 2011 Mw 5.7 earthquake sequence, Geology, 41(6), 699–702, 2013.

Keranen, K. M., Weingarten, M., Abers, G. A., Bekins, B. A. and Ge, S.: Sharp increase in central Oklahoma seismicity since 2008 induced by massive wastewater injection, Science, 25, 448–451, 2014.

Kerner, K. R.: Permeability architecture of faulted nonconformities: Implications for induced seismicity, New Mexico Institute of Mining and Technology., 2015.

Lemen, D., Lindline, J. and Bosbyshell, H.: The Gallinas Canyon gneiss: a window into the nature and timing of Paleoproterozoic events in Northern New Mexico, Geology of the Las Vegas Region., 2015.

Lewan, M. D.: Metasomatism and weathering of the Presque Isle serpentinized peridotite, Marquette, Michigan [MS thesis],
340 1972.

Marshak, S., Domrois, S., Abert, C., Larson, T., Pavlis, G., Hamburger, M., Yang, X., Gilbert, H. and Chen, C.: The basement revealed: Tectonic insight from a digital elevation model of the Great Unconformity, USA cratonic platform, Geology, 45(5), 391–394, doi:10.1130/G38875.1, 2017.

Mossler, J. H.: Geologic Atlas of Fillmore County, Minnesota, University of Minnesota., 1995.

345 Murray, W. E.: Class II Saltwater Disposal for 2009–2014 at the Annual-, State-, and County- Scales by Geologic Zones of Completion, Oklahoma, Oklahoma Geological Survey, Oklahoma., 2015.

Nicholson, C. and Wesson, R. L.: United States Geological Survey, Alexandria, VA., 1990.

Oliver, N. H. S., McLellan, J. G., Hobbs, B. E., Cleverly, J. S., Ord, A. and Feltrin, L.: Numerical models of extensional deformation, heat transfer, and fluid flow across basement-cover interfaces during basin-related mineralization, Economic
350 Geology, 101(1), 1–31, 2006.

Ortiz, J. P.: The role of fault-zone architectural elements and basal altered zones on downward pore pressure propagation and induced seismicity in the crystalline basement, New Mexico Institute of Mining and Technology, Socorro, New Mexico, USA., 2017.

Ortiz, J. P., Person, M. A., Mozley, P. S., Evans, J. P. and Bilek, S. L.: The role of fault-zone architectural elements on pore
355 pressure propagation and induced seismicity, Groundwater, 57, 465–478, doi:10.1111/gwat.12818, 2019.

Petersen, M. D., Mueller, C. S., Moschetti, M. P., Hoover, S. M., Llenos, A. L., Ellsworth, W. L., Michael, A. J., Rubinstein, J. L., McGarr, A. F. and Rukstales, K. S.: 2016 One-year seismic hazard forecast for the Central and Eastern United States from induced and natural earthquakes., 2016.

Rojstaczer, S. A. I. S. E. H. D. O.: Permeability of continental crust influenced by internal and external forcing, Geofluids,
360 8(2), 128–139, 2008.

Segall, P. and Lu, S.: Injection-induced seismicity: Poroelastic and earthquake nucleation effects, Journal of Geophysical Research, 120, 5280–5103, 2015.

Sims, P. K.: Precambrian Basement Map of the Northern Midcontinent, U.S.A., 1990.

Sloss, L. L.: Sequences in the cratonic interior of North America., 1963.

365 Smith, K., Paulding, A., Bradbury, K., Potter, K., Evans, J. and Petrie, E.: Geologic Characterization of the Great Unconformity Injection Interface Region from Field and Drillcore Analog Studies: Implications for Midcontinent Induced Seismicity, Phoenix, AZ, USA., 2019.

Weingarten, M., Ge, S., Godt, J. W., Bekins, B. A. and Rubinstein, J. L.: High-rate injection is associated with the increase in U.S. mid-continent seismicity, Science, 248(6241), 1336–1340, 2015.

370 Whitmeyer, S. J. and Karlstrom, K. E.: Tectonic model for the Proterozoic growth of North America, Geosphere, 3(4), 220–259, 2007.

Wisconsin Geological Natural History Survey, Data: Porosity and density measurements: https://wgnhs.wisc.edu/maps-data/data/rock-properties/porosity-density-measurements-data/. Accessed August 2019

375 Yehya, A., Yang, Z. and Rice, J. R.: Effect of fault architecture and permeability evolution on response to fluid injection, Journal of Geophysical Research: Solid Earth, 123, 9982–9987, doi:10.1029/2018JB016550, 2018.

Zhang, Y., Person, M., Rupp, J., Ellett, K., Celia, M. A., Gable, C., Bowen, B., Evans, J., Bandilla, K., Mozley, P., Dewers, T. and Elliot, T.: Hydrogeologic Controls on Induced Seismicity in Crystalline Basement Rocks Due to Fluid Injection into Basal Reservoirs, Groundwater, doi:10.1111/gwat.12071, 2013.

380 Zhang, Y., Edel, S. S., Pepin, J., Person, M., Broadhead, R., Ortiz, J. P., Bilek, S. L., Mozley, P. and Evans, J. P.: Exploring the potential linkages between oil-field brine reinjection, crystalline basement permeability, and triggered seismicity for the Dagger Draw Oil field, southeastern New Mexico, USA, using hydrologic modeling, Geofluids, 16(5), 971–987, 2016.
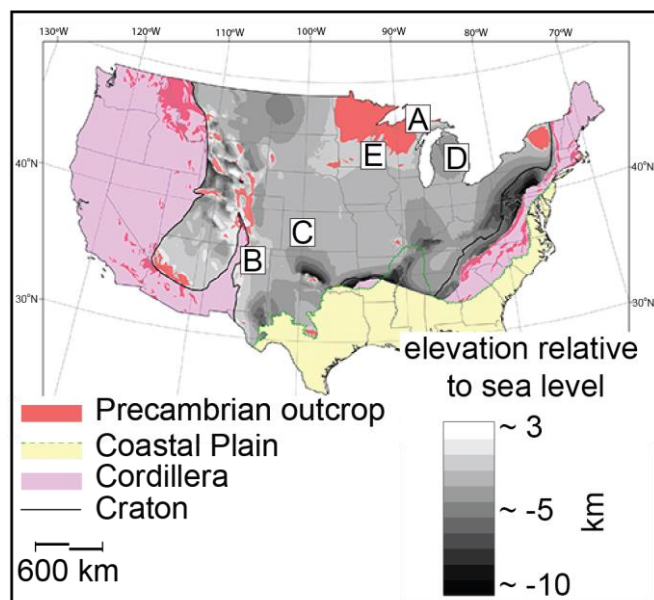
385 **Figure 1. Location of the nonconformity analogue study sites are noted on the top of basement digital elevation model (after Marshak et al., 2017). A) Lake Superior, Presque Isle, Michigan outcrop, B) Gallinas Canyon, New Mexico outcrop C) R.C. Taylor 1 core D) CPC BD-139 core E) BO-1 core.**
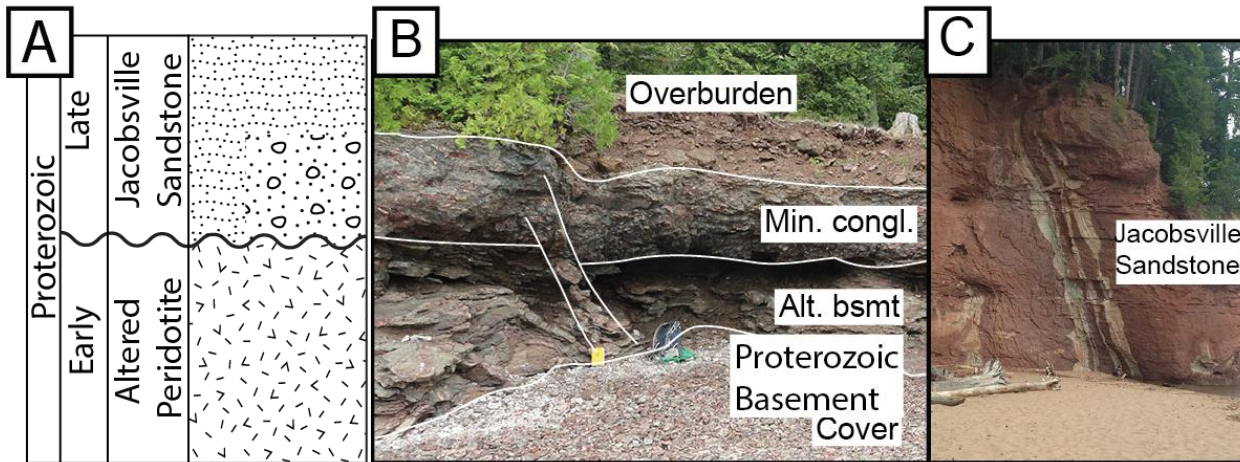
**Figure 2. Lake Superior Michigan Outcrops B) Presque Isle and C) Hidden Beach outcrops. At this locality the Jacobsville Sandstone**
390  **overlies the Proterozoic altered peridotite basement rocks.**
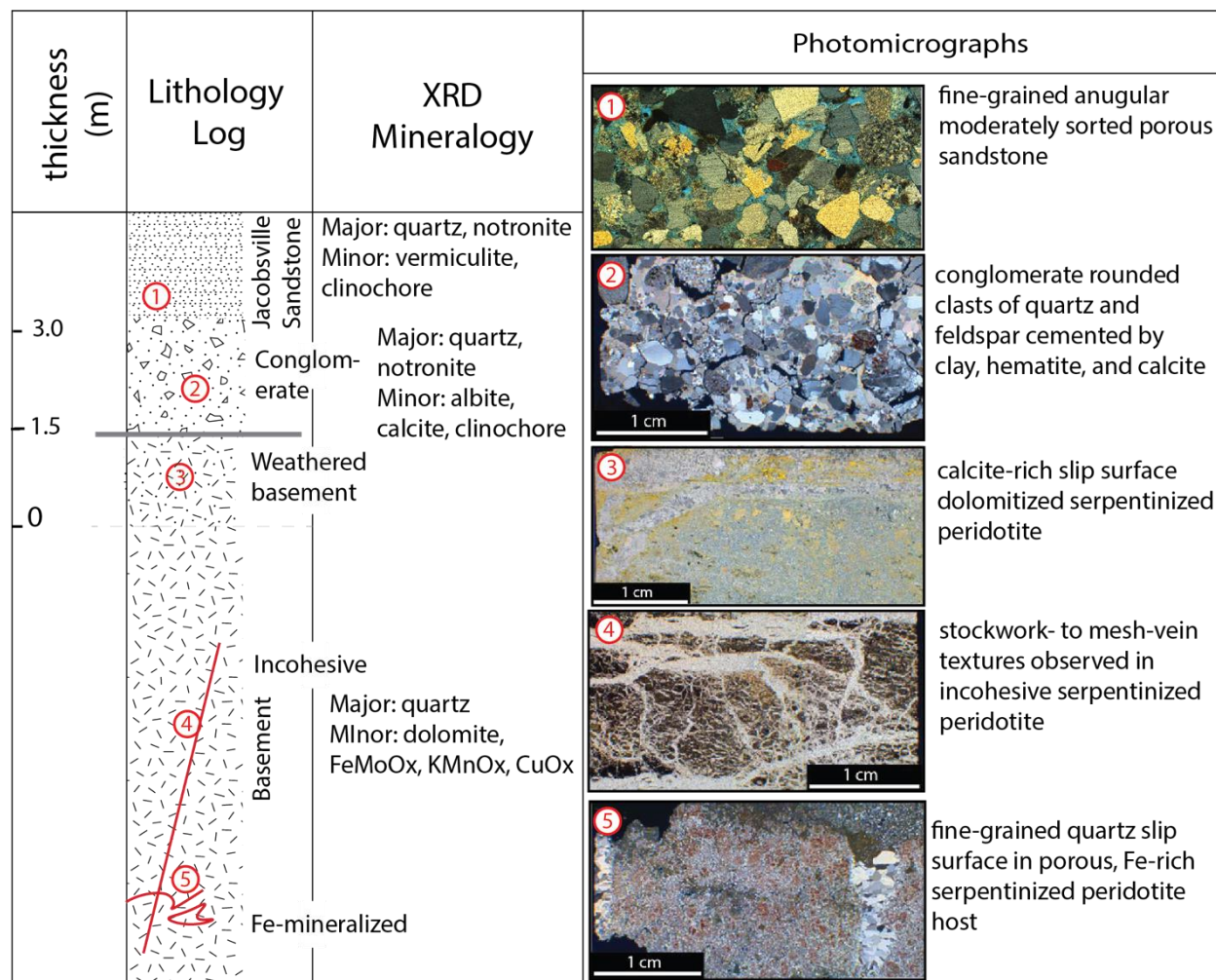
**Figure 3. Petrographic summary figure, photomicrographs and X-ray diffraction results of nonconformity units studied at Presque Isle, Michigan. 1) Jacobsville Sandstone arenite (100x, ppl) 2) Jacobsville Sandstone altered conglomerate (200x, ppl), 3) Basement calcite-rich slip surface in dolomitized, serpentinized peridotite (200x, xpl), B) Basement serpentine (100x, ppl), C) Basement slip surface within cataclasis and associated colloform mineralization (100x, ppl), D) Basement vein assemblages (200x, xpl).**
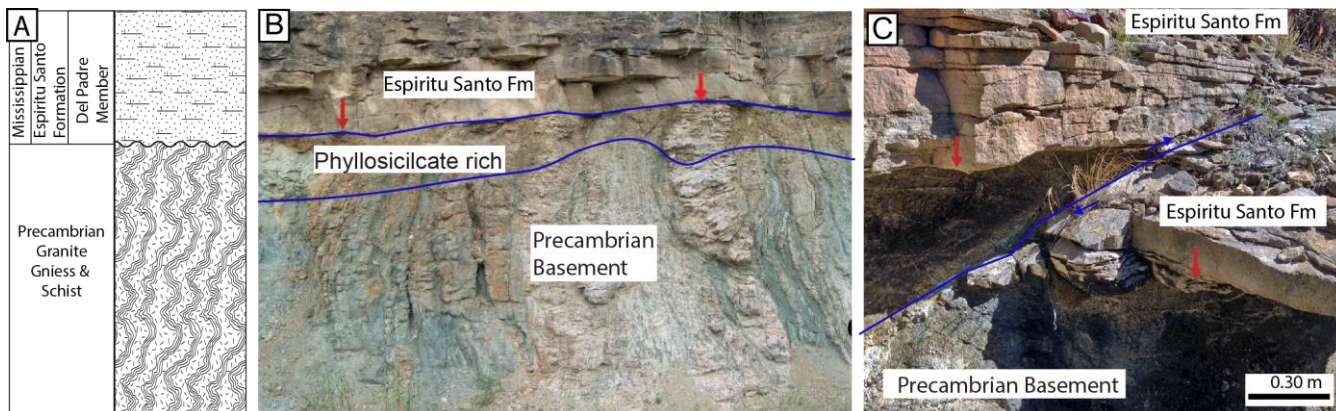
**Figure 4. Gallinas Canyon, New Mexico outcrop, Precambrian granitic gneiss and schist is overlain by the Mississippian Espiritu Santo Formation. The 4 km long exposure in Gallinas Canyon, the nonconformity is cut by several cm- to m- displacement faults (C).**

400
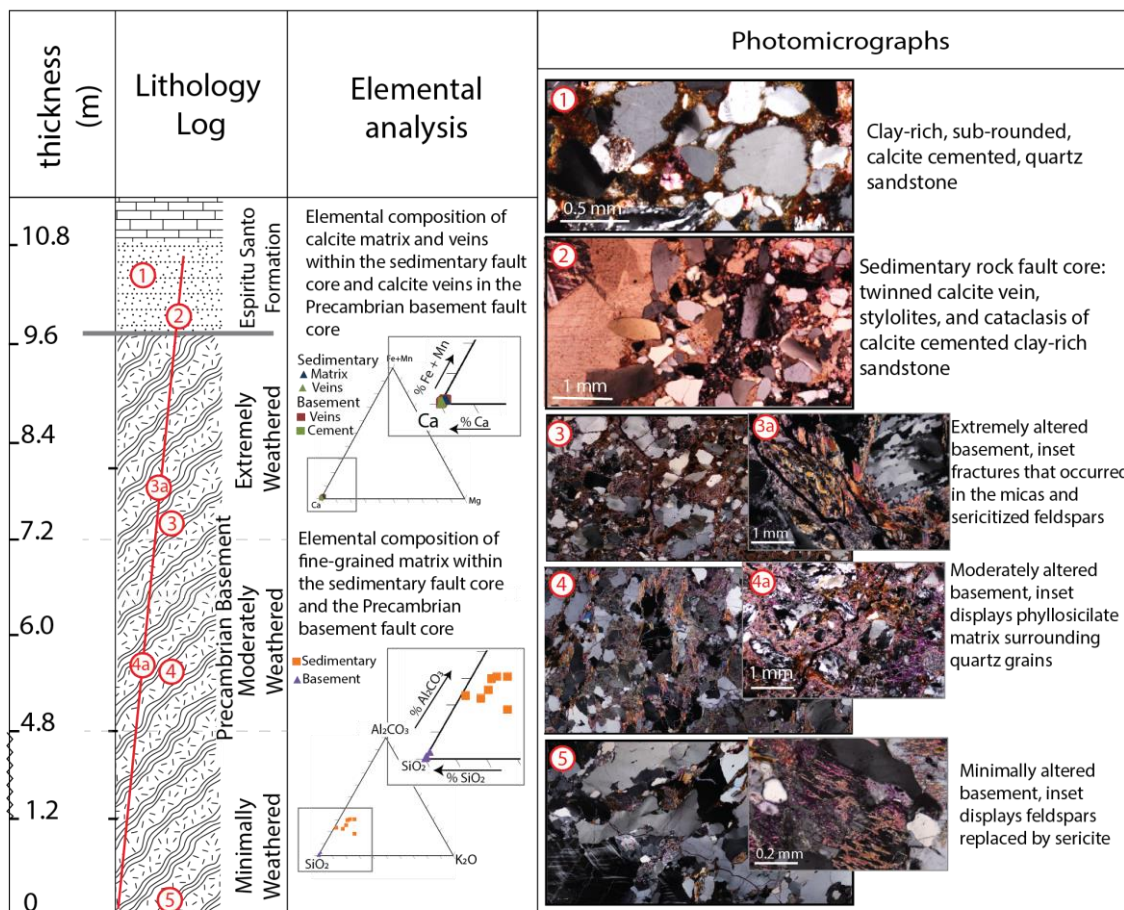
**Figure 5. Petrographic and elemental analysis summary of nonconformity units at Gallinas Canyon site. Elemental analysis shows similar calcite composition of the veins within the sedimentary sequence and the Precambrian basement faults. 1 & 2) The Espirutu Santo sandstones are clay rich calcite cemented quartz sandstones, in the fault core (2) the sandstones are cut by twinned calcite veins and stylolitic textures and contact cataclastic; 3) adjacent to the nonconformity the granitic basement contain fractures in the micas and sericitized feldspars; 4) & 5) basement alteration decreases away from the nonconformity with phyllosilicate matrix surrounding quartz grains and sericitization of feldspars occurring 10 m from the nonconformity.**
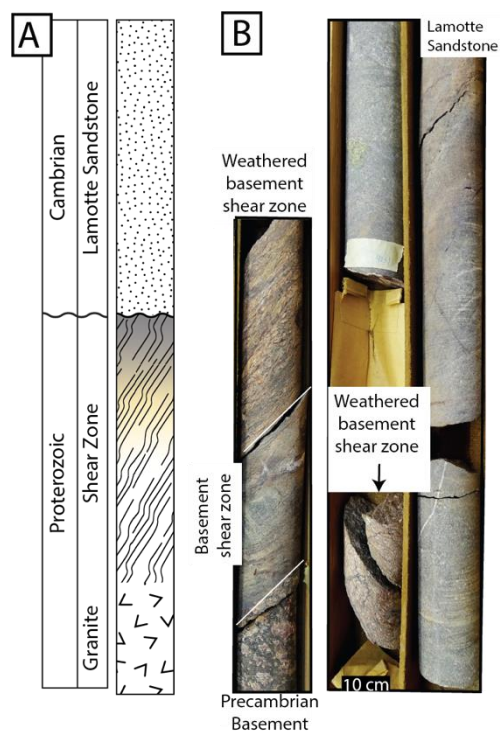
**Figure 6. A) Lithologic log of the R.C. Taylor 1 core, Nebraska, core from 3984-4038' (1214-1231 m) was described. The nonconformity occurs at 4018' MD (1225 m). Four main lithologic units were defined in the core, including sandstone, sedimentary rock hosted shear zone, altered basement shear zone, minimally altered basement. The nonconformity occurs within a shear zone and is cut by thoroughgoing veins.**
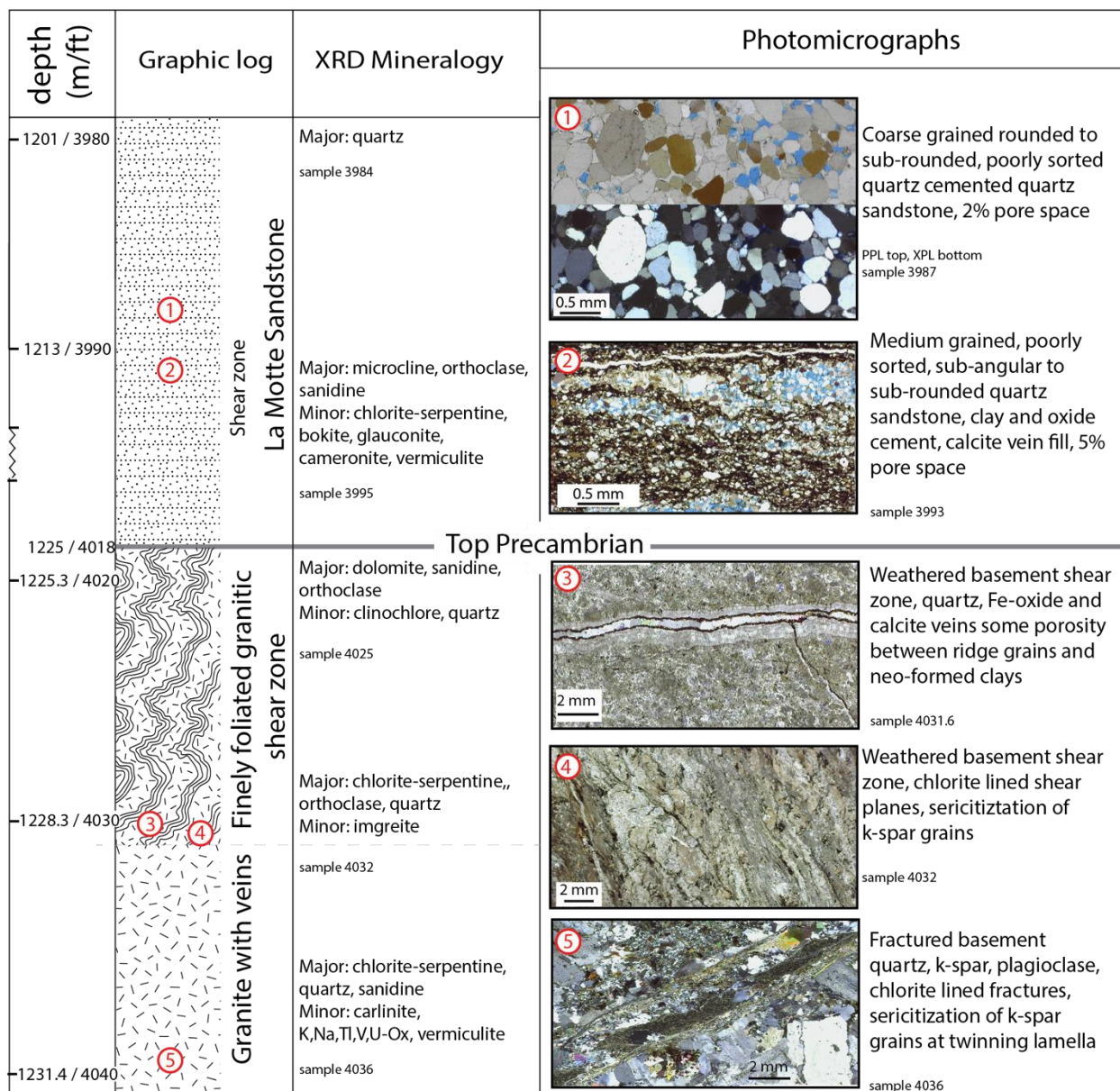
**Figure 7. Petrographic summary figure, photomicrographs and X-ray diffraction results of nonconformity units studied in the R.C.**
**Taylor 1 core; 1) Lamotte Sandstone, rounded to sub-rounded, poorly sorted quartz sandstones (100x, ppl & xpl); 2) lower Lamotte**
**Sandstone, opaque Fe-oxide cements and vein fill, porosity shown by blue epoxy, (100x ppl); 3) Top Precambrian crystalline altered**
**basement shear zone. Syntaxial veins mineralized with quartz, reactivated and mineralized with Fe-oxide then sparry calcite. Some**
**porosity between rigid grains and neo-formed clays (50x PPL); 4) Altered basement shear zone, chlorite lined shear planes,**
**sericitization of feldspars along twining lamella (100x ppl); 5) Coarse crystalline sericitization of feldspars adjacent to twin lamellae**
**(150x XPL).**
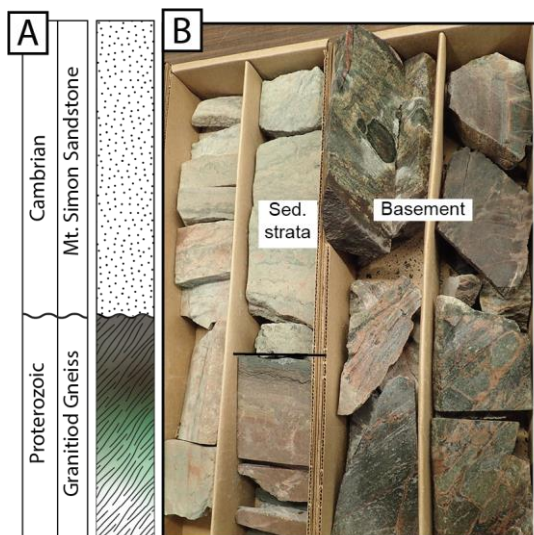
**Figure 8. A) Lithologic log of the CPC BD-139 core, Michigan from 1404-1412.1 meters depth. Five main lithologic units were identified, including sandstone, dolomitized and undolomitized finely foliated gneiss, and dolomitized and undolomitized gneiss with sub-horizontal white veins. B) Photographs of the CPC BD-139 core. Core between ~1404.5-1405.5 meters. Contact between the Cambrian Mt. Simon Sandstone (light tan) and the underlying Precambrian gneiss. The gneiss directly at the contact is fine-grained, tan, and dolomitized. This is underlain by green altered gneiss with sub-vertical pink-coated fractures. This lithology grades into a dark grey gneiss with sub-horizontal white veins (core between 1411.5-1412.5 meters), which extends through the bottom of the logged section.**
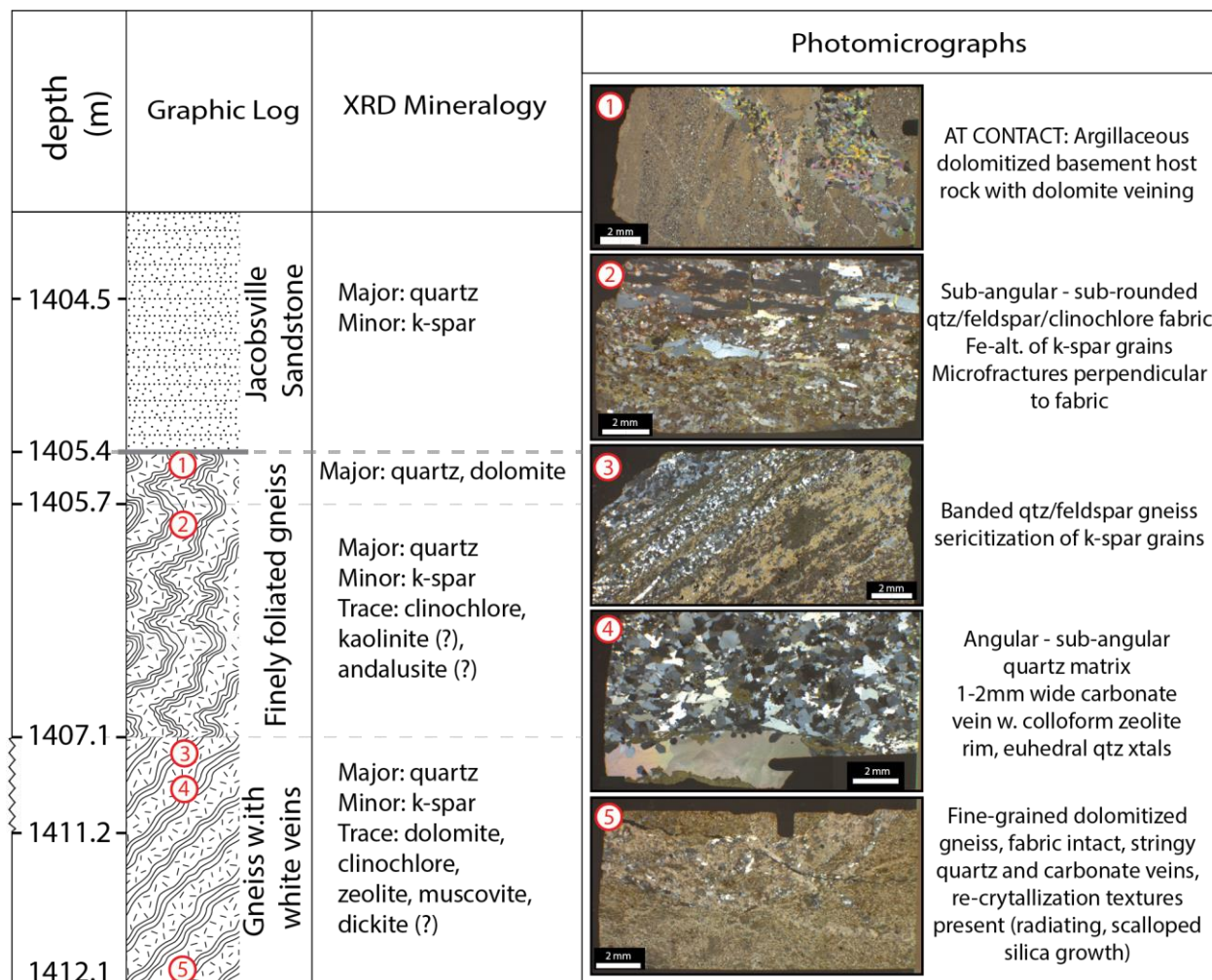
**Figure 9. Petrographic summary figure, photomicrographs and X-ray diffraction results of nonconformity units studied in CPC BD-139 core. 1) Basement sample at the contact is an argillaceous dolomitized gneiss whit dolomite veins (XPL); 2) Foliation defined by quartz-feldspar-clinochore fabric with iron alteration of potassium feldspar grains (XPL); 3) banded quartz-feldspar gneiss with common sericitization of potassium feldspar grains (XPL); 4) Carbonate vein with colloform zeolite rim and euhedral quartz crystals (XPL); 5) dolomitized gneiss with common quartz and carbonate veins (XPL).**
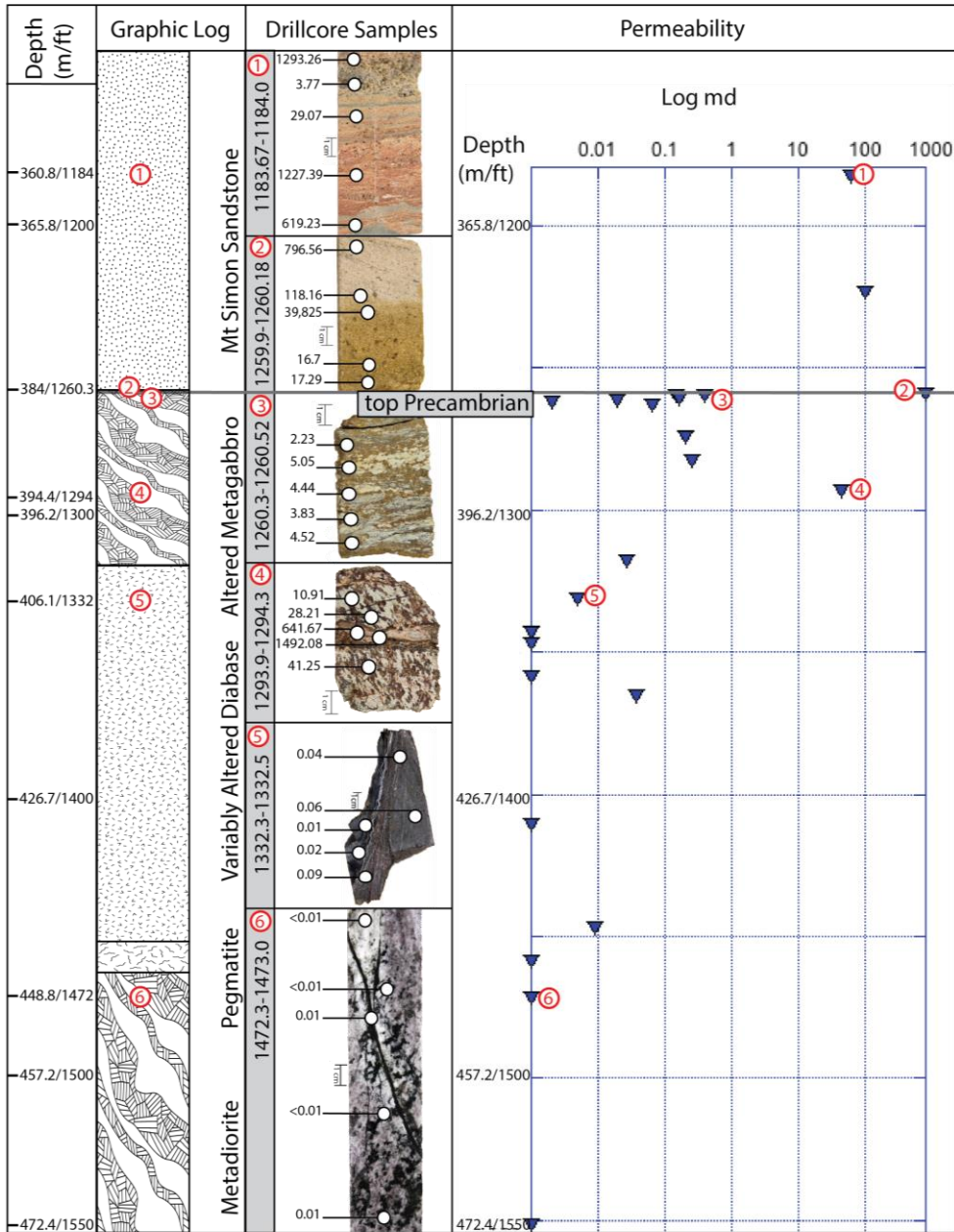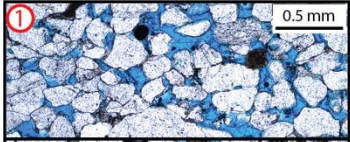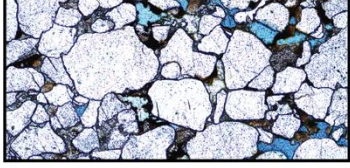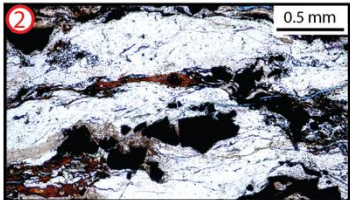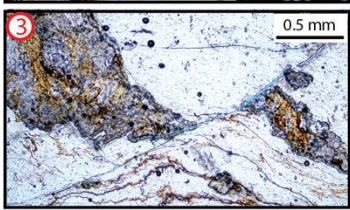
**Figure 10. BO-1 lithologic log with select representative core samples of each the major lithologic units shown. Above the nonconformity, the analogue reservoir or injection unit, the Cambrian Mt. Simon Sandstone is porous with evidence for both dissolution and oxidation front. The crystalline basement rock consists of foliated, intensely altered and altered metagabbro with localized faulting, variably altered and faulted diabase, localized pegmatite dikes, and relatively unaltered and less-deformed metadiorite. Gas permeability measurements were made on 25 core samples spanning the nonconformity interface. For each core**

435

440

**sample tested, 5 spot measurements were made (locations shown by white circles). For relative comparison across the contact and within the various lithologic units, data is plotted using a log scale and the averaged values for each sample.**

| Depth (m/ft) | Graphic Log | | XRD Mineralogy | Photomicrographs |
|---|---|---|---|---|

**Mt Simon Sandstone**

- 365.8/1200

Major: quartz
Minor: Fe-oxides

Major: quartz, Fe-oxides
Minor: Fe-hydroxide (goethite)

**①** 0.5 mm — fine- to medium-grained, subangular to subrounded, well-sorted porous sandstone

iron-coated and irregularly cemented, siderite crystals partially fill pore space

Sample: 1259.9-1260.18

**Nonconformity contact**

- 384/1260.3   ① ② ③

**Altered Metagabbro**

Major: Fe-hydroxide (goethite), Mn-oxides, Fe-oxides, magnesio-chloritoid (ferroan)
Minor: ankerite, dolomite

- 394.4/1294   ④
- 396.2/1300
- 398/1305.9   ⑤

HOST
Major: dolomite, Ti-oxide (anatase)
Minor: ramsbeckite
SLIP
Major: dolomite, birnessite, Mo-oxide, quartz, nacrite clay (kaolinite-serpentine)

**②** 0.5 mm — strongly weathered, meta-gabbro-norite intensely altered ~ 60 m dolomitization

Sample: 1260.3-1260.52

**③** 0.5 mm — argillization-alteration along discrete discontinuties

mutliple cm - micrometer scale slip surfaces

Sample: 1260.52-1261.25

**Variably Altered Diabase**

- 406.1/1332   ⑥

Major: Fe-oxides, Cu-hydroxides (clinoclase), muscovite, illite

- 426.7/1400

HOST
Major: siderite, dolomite, adularia minor: Fe-rich smectite (nontronite)

HOST
Major: diopside, clinochlore (Fe-rich)
Minor: Mn-oxides, andsesine, ramsbeckite
SLIP
Major: quartz, Fe-oxides
Minor: fluorapatite, zeolites, Mn-oxides

**④** 0.5 mm — argillization-alteration extends outward from fracture surfaces

open fractures

Sample: 1293.9-1294.3

**⑤** 0.5 mm — multi-layered vein, slip surface dilational pull-apart micro-structures
crack-seal textures serpentinization, dolomitization

Sample: 1305.85-1305.95

**⑥** 0.5 mm — multi-layered shear zone of multi-phase composition

anastomosing and cross-cutting vein textures

Sample: 1332.3-1332.5

**Pegmatite**

**Metadiorite**

- 448.8/1472   ⑦

Major: albite (Ca), anorthite,
Minor: calcite, ferro-actinolite, vermiculite, Na-Ca plagioclase (andesine)

- 457.2/1500

**⑦** 0.5 mm — moderately altered feldspars

ultracataclasite along mm-scale shear zones

Sample: 1472.3-1473

**Figure 11. X-ray Diffraction mineralogy and photomicrographs of BO-1 drill core samples showing representative compositions and**

445 **textures across the non-conformity interface contact. Samples within centimetres of the contact (1-3) are strongly weathered, altered,**

**and slightly metamorphosed gabbro-norite. Alteration and diagenesis assemblages include Iron-oxides-hydroxides with chlorite,**

**ankerite, and dolomite. Alteration extends for ~ 50 m into the basement. Sample 3 illustrates mm-scale offset across argillite layer.**

**Note fracture permeability (blue-epoxy) parallel to slip surface. Fracture surfaces within Sample 4 at 34 m below the contact are**

**several mm's of mixed chlorite-clay alteration and fine-scale permeability (blue-epoxy). Sample 5 at 1304.9 m shows multiple phases**

450 **of fluid-rock interactions coupled with dilation, serpentinization, and dolomitization. Multi-layered clay-rich fault core gouge within**

**Sample 6 at 1332 m or ~ 70 m below the contact. Note, open fractures within central portion of fault core gouge (blue-epoxy). At**

**1472 m or 272 m below the contact within the meta-grano-diorite unit, clay alteration is observed within feldspar grains at the micro-**

**scale.**

455
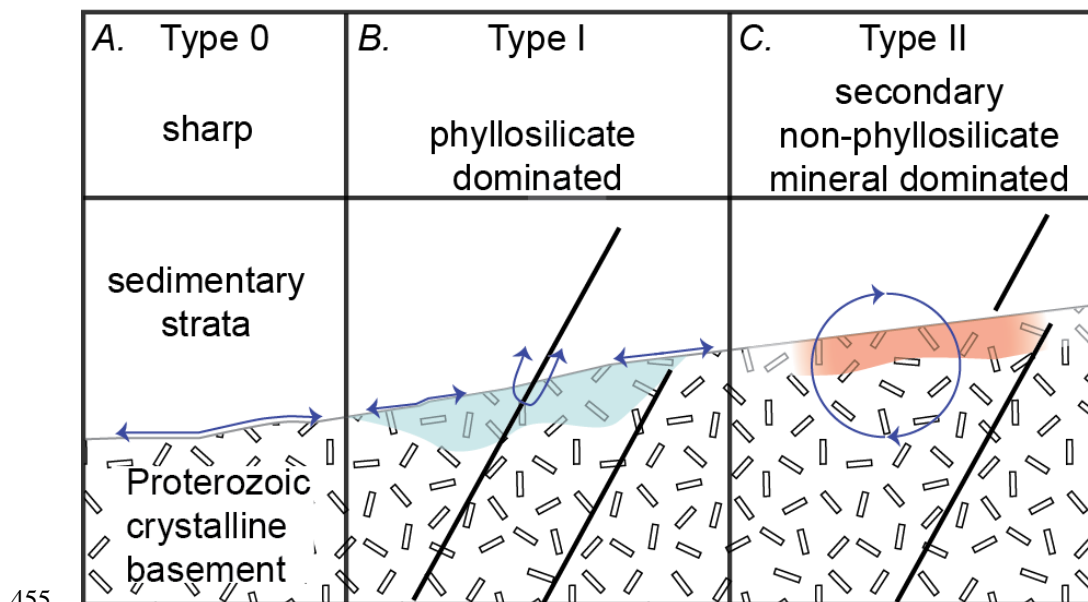
**Figure 12. Proposed geologic schematics of the non-conformity contact region. A. Type 0 – sharp contact; B. Type I – weathering**

**dominated zone Proterozoic crystalline basement, C. Type II – secondary mineralization dominated zone. All nonconformity types**

**may be cut by structural discontinuities. Blue arrows indicate potential flow paths of injected fluids.**
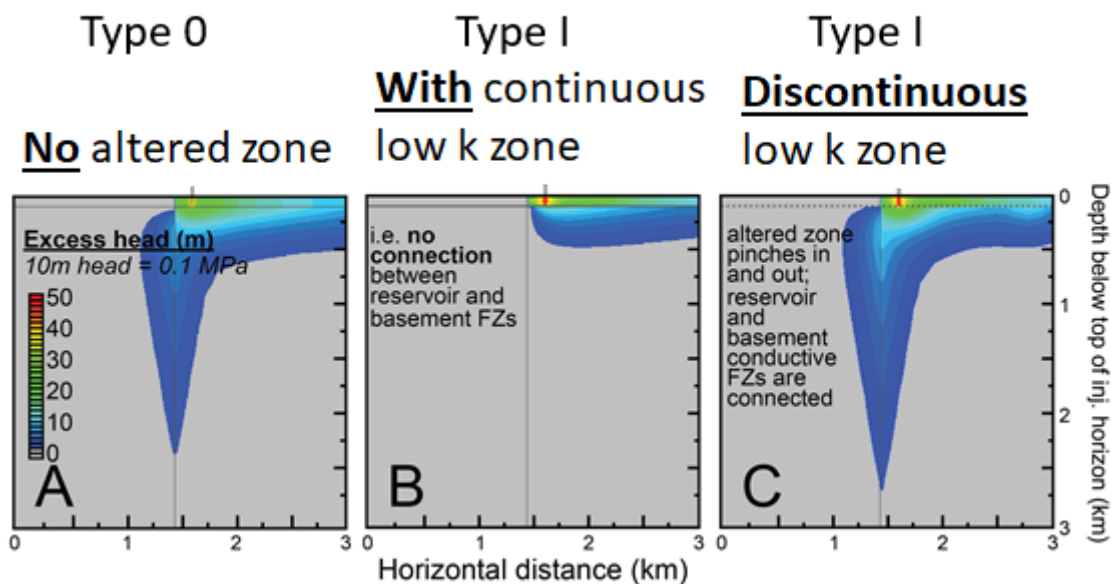
**Figure 13. Cross-sectional views of pore pressure envelope propagation resulting from injection into a reservoir underlain by a low permeability altered zone. Excess hydraulic heads after 4 years of constant-rate injection are presented for a Palaeozoic conduit-barrier fault scenario (A) Type 0 nonconformity, absent a low-permeability altered zone, (B) Type I nonconformity, with an altered zone present as a 20-m-thick confining layer (represented by two horizontal grey lines) that is continuous such that reservoir and basement fault zones do not connect, and (C) Type I nonconformity, with a discontinuous altered zone that pinches in and out in 20-m horizontal intervals (i.e. undulating) but where the reservoir and basement fault zones are fully connected. Results are zoomed in to the top 3 km × 3 km of the model domain. Vertical grey lines indicate location of the fault zone. Injection well location is indicated on top of each panel. Transition from grey to dark blue contour (and all subsequent contour lines) denotes a 2-m increase in hydraulic head (0.02 MPa). Adapted from Ortiz (2017; for details of the modelling approach see Ortiz et al., 2019).**